Electronic Supplementary Information

Studying the effect of Zn-substitution on the magnetic and hyperthermic properties of cobalt ferrite nanoparticles

Valentina Mameli[a,b], Anna Musinu[a,b], Andrea Ardu[a,b,c], Guido Ennas[a,b], Davide Peddis[d], Daniel Niznansky[e], Claudio Sangregorio[b,f], Claudia Innocenti[g,b], Nguyễn T. K. Thanh*[h], Carla Cannas*[a,b,c]

[a]Department of Chemical and Geological Sciences, University of Cagliari, Monserrato (CA), Italy

[b]Consorzio Interuniversitario Nazionale per la Scienza e Tecnologia dei Materiali (INSTM), Italy

[c]Consorzio AUSI, CREATE, Palazzo Bellavista Monteponi, Iglesias (CI), Italy

[d]Istituto di Struttura della Materia, Consiglio Nazionale delle Ricerche (ISM-CNR), Italy

[e]Department of Inorganic Chemistry, Charles University of Prague, Czech Republic

[f]Istituto di Chimica dei Composti OrganoMetallici, Consiglio Nazionale delle Ricerche (ICCOM-CNR), Sesto Fiorentino (FI), Italy

[g]LAboratorio di Magnetismo Molecolare (LA.M.M), Department of Chemistry, University of Florence, Sesto Fiorentino (FI), Italy

[h]Biophysics Group, Department of Physics and Astronomy, University College London, Gower Street, London WC1E 6BT, UK and UCL Healthcare Biomagnetic and Nanomaterials Laboratory, 21 Albemarle Street, London W1S 4BS, UK

Email: ccannas@unica.it, ntk.thanh@ucl.ac.uk

1. ICP-AES analysis

For the ICP-AES analysis, the samples were prepared as follows. Nanoparticles' powders were digested by using aqua regia (3:1 HCl/HNO_3). The digested sample solutions were heated up to ~90 °C for 1 h under magnetic stirring, then to ~200 °C for 10 minutes. The solutions were left to cool down, filtered and diluted by using 1% v/v HNO_3 solution. The ICP measurements were made by means of a Liberty 200 ICP Varian spectrometer using the following spectral lines: Fe line: 259.940 nm, Co line: 228.616 nm, Zn line: 213.856 nm. Taking into consideration the theoretical detection limit specific for the instrument (Fe detection range: (0.015÷750) ppm, Co detection range: (0.050÷2500) ppm, Zn detection range: (0.009÷450) ppm) and the range of linearity, the following range concentrations have been selected for both the standard solutions and samples solutions: Fe concentration range: (0÷1.5) ppm, Co concentration range: (0÷2) ppm, Zn concentration range: (0÷1) ppm. The analyses have been repeated two times on different portions of the samples. The chemical formulas were calculated by assuming the absence of anions vacancies.

Figure S1. XRD patterns of the CoFe_Znx (with x=0, 0.30, 0.46, 0.53) samples recorded by a PANalytical X'Pert PRO powder X-ray diffraction system equipped with a Co Kα source (λ=1.78901 Å) and an X'Celerator detector.

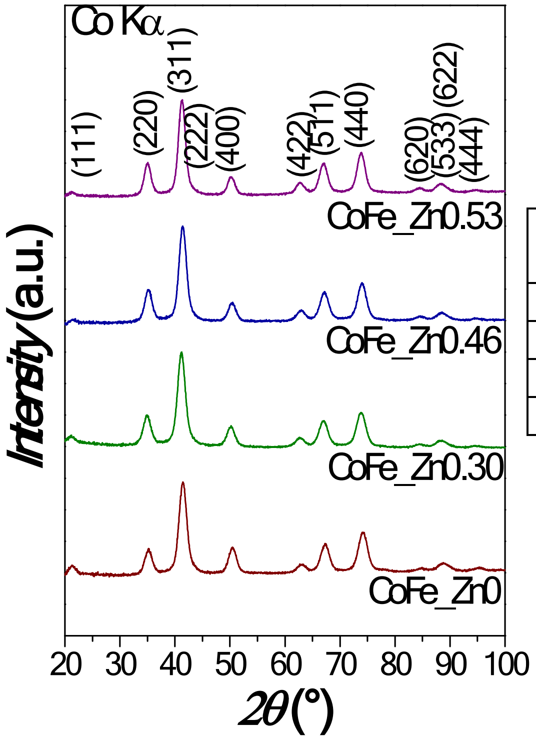

Sample	**$\langle D_{XRD}\rangle_{CuK\alpha}$ (nm)**	**$\langle D_{XRD}\rangle_{CoK\alpha}$ (nm)**
CoFe_Zn0	6.1±0.3	6.0±0.1
CoFe_Zn0.30	5.9±0.2	5.8±0.1
CoFe_Zn0.46	6.0±0.3	6.0±0.2
CoFe_Zn0.53	6.7±0.4	6.6±0.2

Table S1. Lattice constant and cationic distribution obtained by Rietveld analysis (performed on the Cu-XRD patterns) for the CoFe_Znx (with x=0, 0.30, 0.46, 0.53) samples. The last column lists the indexes of agreement.

Sample	***a* (Å)**	**Cationic distribution**	**R (%)**
CoFe_Zn0	8.390(2)	$(Fe_{0.73}Co_{0.27})[Fe_{1.26}Co_{0.74}]O_4$	5.79
CoFe_Zn0.30	8.414(2)	$(Fe_{0.38}Co_{0.42}Zn_{0.20})[Fe_{1.62}Co_{0.28}Zn_{0.10}]O_4$	6.19
CoFe_Zn0.46	8.418(2)	$(Fe_{0.30}Co_{0.44}Zn_{0.26})[Fe_{1.70}Co_{0.10}Zn_{0.20}]O_4$	6.12
CoFe_Zn0.53	8.433(2)	$(Fe_{0.28}Co_{0.39}Zn_{0.33})[Fe_{1.72}Co_{0.08}Zn_{0.20}]O_4$	6.50

A raw estimation of the distribution of the metallic cations in the tetrahedral and octahedral sites has been attempted. It is worth noting that iron, cobalt and zinc are characterised by similar X-ray scattering factors values and, therefore, these cationic distributions have to be considered just as general tendencies. Nevertheless, these data suggest that the samples are characterised by partially inverse structures: the cobalt ferrite sample seems to have an inversion degree of about 0.70, which is a value often reported in the literature for cobalt ferrite nanoparticles.[1–3] When zinc ions replace cobalt ones within the structure, the inversion degree seems to drop down. This again suggests a 4-fold coordination of zinc ions, that forces iron ones to occupy octahedral sites.

Figure S2. Intensity ratio of different XRD reflections for the CoFe_Znx (with x=0, 0.30, 0.46, 0.53) samples with the corresponding linear curve fitting.

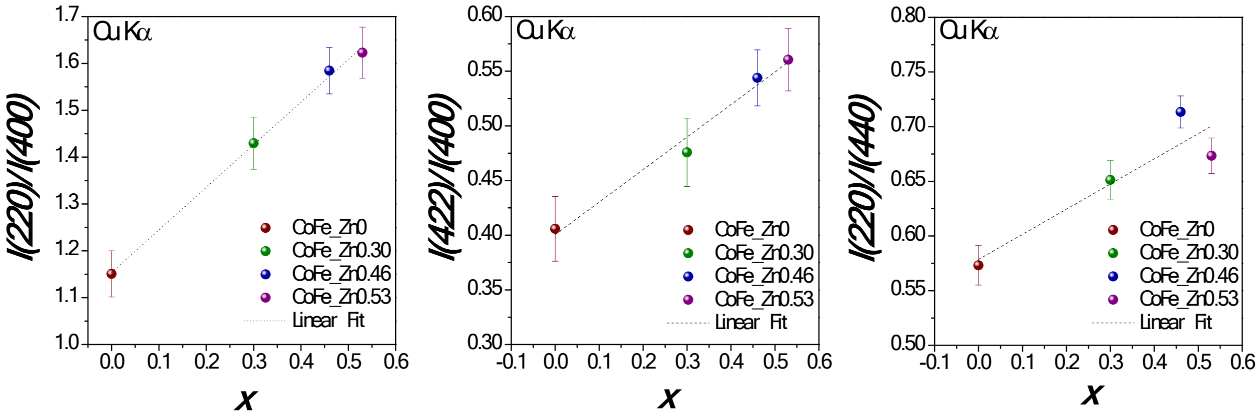

I(220)/I(400): $y = 1.15377 + 0.90921x$ (R^2=0.99637)

I(422)/I(400): $y = 0.40054 + 0.29759x$ (R^2=0.97261)

I(220)/I(440): $y = 0.57855 + 0.23024x$ (R^2=0.76687)

The intensity ratio between the (220) and the (400) reflections is considered to be sensitive to the cations occupancies of the tetrahedral sites[4–6]. A curve fitting confirms that this ratio linearly increases with increasing zinc content suggesting that the zinc ions substitute cobalt ones by occupying preferentially tetrahedral sites.

Figure S3. TEM images (a) and size distributions of the CoFe_Znx (with x=0, 0.30, 0.46, 0.53) samples obtained by means of JEOL JEM-1200 EX II TEM. (c) Mean particle sizes and polydispersity indexes obtained by different microscopes.

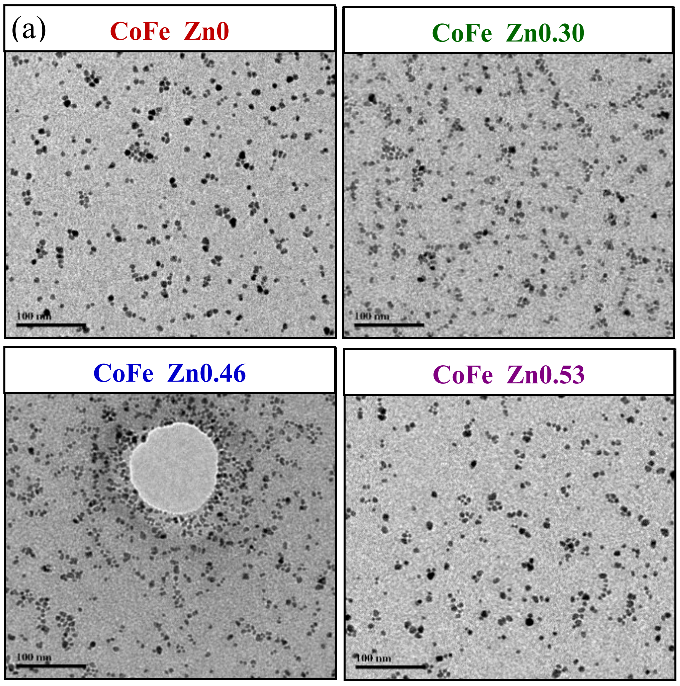

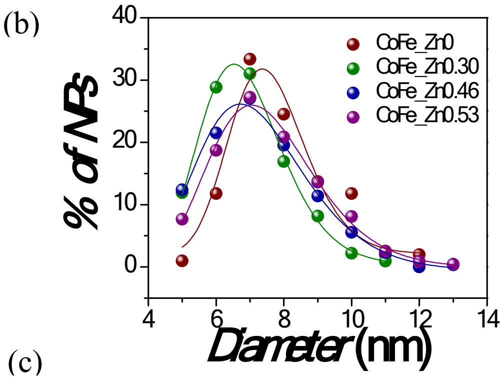

(c)

Sample	$\langle D_{TEM} \rangle$ (nm)*	σ (%)*	$\langle D_{TEM} \rangle$ (nm)**	σ (%)**
CoFe_Zn0	7.5±1.7	22	7.7±1.4	18
CoFe_Zn0.30	7.1±1.4	19	6.9±1.2	18
CoFe_Zn0.46	7.3±1.6	22	7.3±1.5	22
CoFe_Zn0.53	8.0±1.9	24	7.6±1.6	21

* JEM 2010 UHR

** JEOL JEM-1200 EX II

Figure S4. (a) FT-IR spectra of the CoFe_Znx (with x=0, 0.30, 0.46, 0.53) samples and (b) assignments of the most relevant vibrational modes.

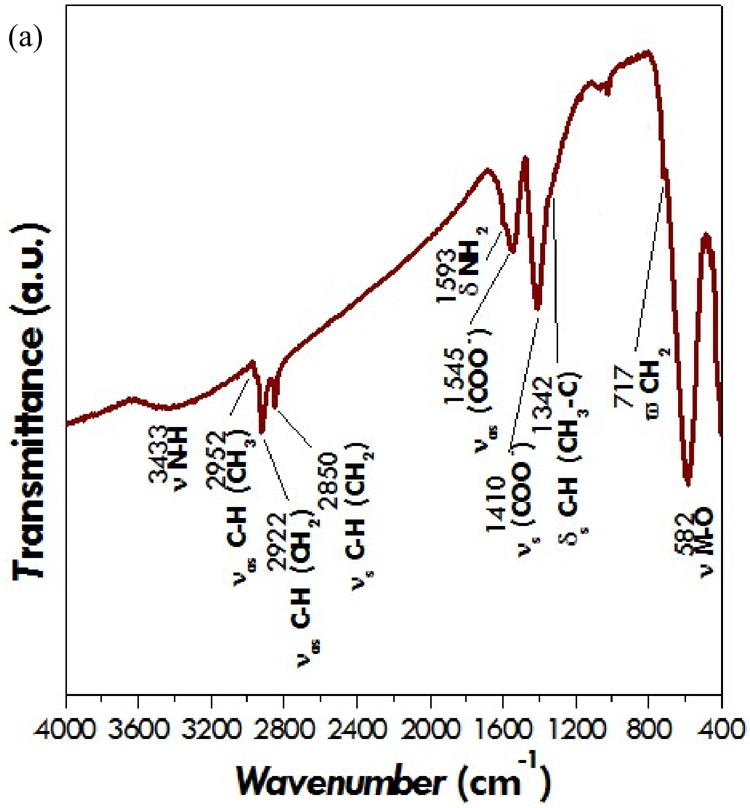

(b)

Wavenumber (cm^{-1})				**Vibrational mode**
CoFe_Zn0	**CoFe_Zn0.30**	**CoFe_Zn0.46**	**CoFe_Zn0.53**	
3433	3400	3371	3408	N-H stretching
2952	2954	2952	2950	C-H asymmetric stretching (CH_3)
2922	2924	2924	2925	C-H asymmetric stretching (CH_2)
2850	2873	2852	2854	C-H symmetric stretching (CH_2)
1593	1595	1593	1592	NH_2 bending
1545	1550	1548	1541	COO^- asymmetric stretching
1410	1415	1414	1415	COO^- symmetric stretching
1342	1340	1346	1340	CH_3 bending
717	719	717	-	CH_2 wagging
582	577	571	569	Metal-O stretching

The FT-IR spectra show the same vibrational modes for all the samples, indicating the presence of the same capping agent. Besides the metal-O stretching at (582÷569) cm^{-1}, the observed vibrational modes are typical for the oleyl (C_{18}) chain (CH stretching, CH_3 bending, CH_2 wagging), the amine (NH stretching, NH_2 bending) and the carboxylate groups (asymmetric and symmetric COO^- stretching). The presence of these latter peaks and their wavenumber difference suggest the presence of bridging monodentate carboxylate bonded to the nanoparticle surface[7]. In addition, the presence of pure oleylamine is indicated by the associated NH_2 vibrational modes[8]. According to these results and previous works[8–11], we can consider the oleic acid as the only capping agent for all the samples whereas a few amine molecules are probably present as intercalated molecules. Moreover, the FT-IR analysis confirms the substitution of cobalt ions by zinc ones within the spinel structure. Indeed, the metal-oxygen stretching mode moves from 582 cm^{-1} for the $CoFe_2O_4$ towards lower wavenumber values (569 cm^{-1} for $Zn_{0.53}Co_{0.47}Fe_{2.0}O_4$) with increasing zinc content as expected being the positions of this band at 575 cm^{-1} and 555 cm^{-1} for the cobalt and zinc ferrites, respectively.[12]

Figure S5. (a) ThermoGravimetric curves of the CoFe_Znx (with x=0, 0.30, 0.46, 0.53) samples; (b) first derivative of the ThermoGravimetric curves (DTG).

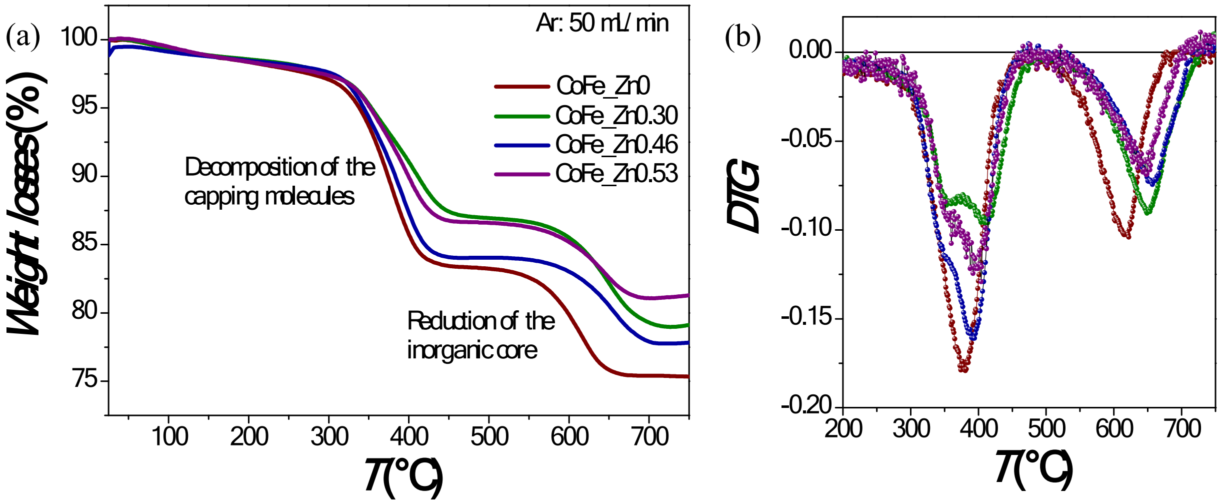

TGA curves show two weight losses occurring at (300÷400) °C and (550÷650) °C that can be associated with the decomposition of the capping molecules and a reduction process of the inorganic core that occurs only when the thermogravimetric analysis is conducted under argon atmosphere as already observed by other authors for oleic acid-capped zinc ferrite nanoparticles[13]. TGA enable us to determine a mean organic content of (15 ± 2) %. It can be easily demonstrated that this amount of capping agent corresponds to a low-dense packing of a monolayer of oleate molecules surrounding the surface of the nanoparticles. Indeed, for a close-packed monolayer the expected area occupied by a single oleate molecule on the nanoparticle surface is around 20-30 Å^2.[14–16] In our case, considering a mean diameter of 7.5 ± 0.4 nm and a spheroidal shape for the NPs, a surface area of 177 nm^2 is obtained. A 15 ± 2 % of organic capping corresponds to ~$3.2\cdot10^{20}$ oleate molecules. Taking into account the *bulk*-$CoFe_2O_4$ density of 5.3 g/cm^3 and the volume of a single spheroidal NP with a diameter of 7.5 nm, an 85% of inorganic phase corresponds to a number of spinel ferrite NPs of $7.1\cdot10^{17}$. The number of capping molecules per particle, obtained as the ratio between the number of oleate molecules and the number of NPs should, is about 440 molecules/nanoparticle. Finally, the nanoparticle surface area (177 nm^2) over the number of molecules provides a surface area occupied by each oleate molecule of 39 Å^2.

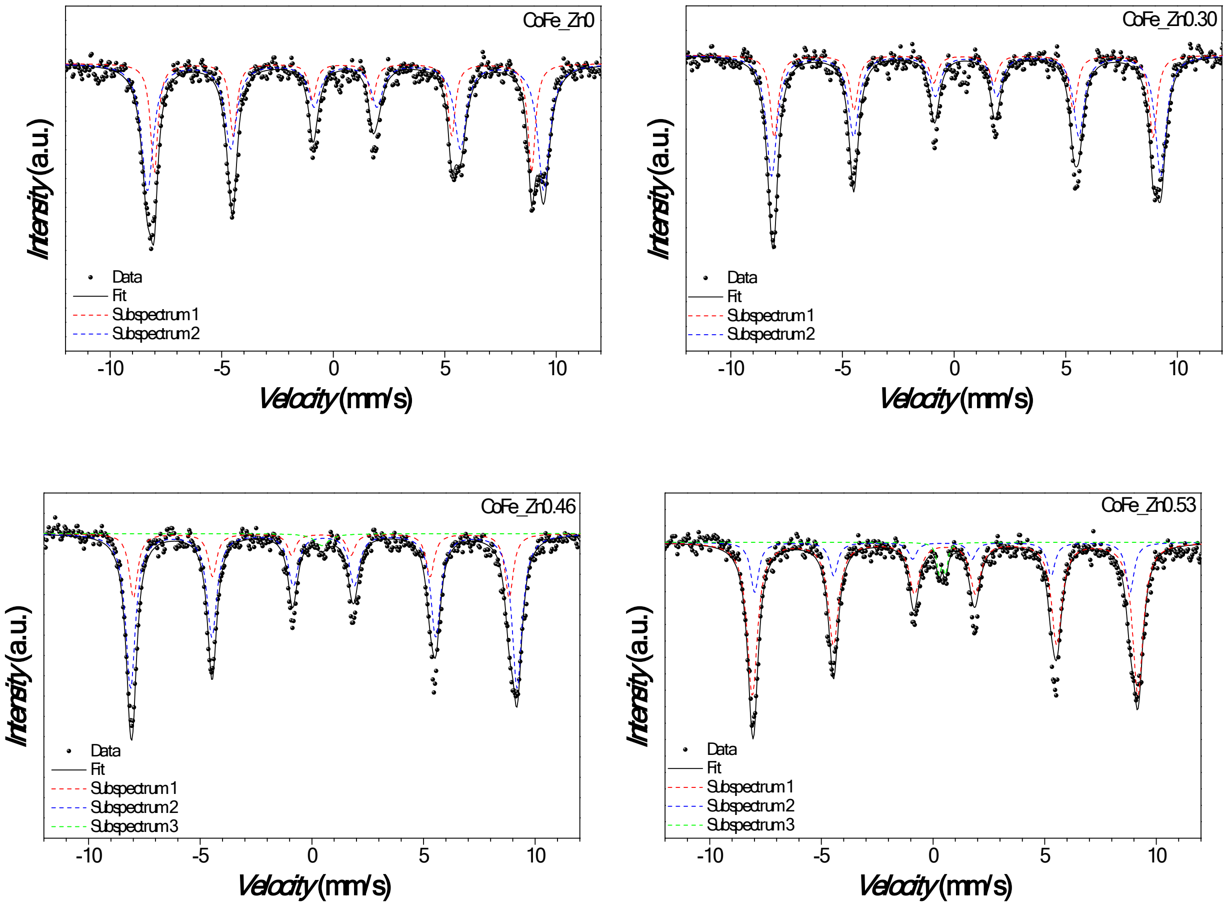

Figure S6. Mössbauer spectra of the CoFe_Znx (with x=0, 0.30, 0.46, 0.53) samples at 4.2 K under zero magnetic field (0 T). Note that the doublet in the centre of the spectra is related to the metallic iron dissolved in the aluminium foil (sample holder).

Table S2. Mössbauer parameters of the CoFe_Znx (with x = 0, 0.30, 0.46, 0.53) samples at 4.2 K under intense magnetic field (6 T): values of isomer shift (δ), quadrupole splitting (ΔE_Q), effective magnetic field (B_{Hf}), Full width at half maximum (FWHM) and relative area (A) of the components. The last column lists the cationic distribution.

Sample	**Subsp.**	**δ (mm/s)**	**ΔE_Q (mm/s)**	**B_{Hf} (T)**	**FWHM [mm/s]**	**Interpretation**
CoFe_Zn0	1	0.42	0.02	52.6(3)	0.40	tetrahedral sites of a spinel
	2	0.56	0.00	55.2(3)	0.64	octahedral sites of a spinel
CoFe_Zn0.30	1	0.43	0.00	52.7(3)	0.43	tetrahedral sites of a spinel
	2	0.54	0.00	54.1(3)	0.58	octahedral sites of a spinel
CoFe_Zn0.46	1	0.42	0.00	52.3(3)	0.45	tetrahedral sites of a spinel
	2	0.54	0.00	53.8(3)	0.54	octahedral sites of a spinel
CoFe_Zn0.53	1	0.42	0.00	52.2(3)	0.43	tetrahedral sites of a spinel
	2	0.54	0.00	53.6(3)	0.56	octahedral sites of a spinel

Table S3. The in-field measurements were done in a perpendicular arrangement of the external magnetic field with respect to the γ-beam and are useful to get information about the cationic distribution and the canting phenomena in the spinel structure.

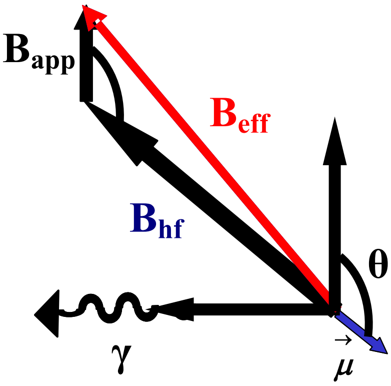

Indeed, the angle θ between the magnetic moment ($\vec{\mu}$) and the applied magnetic field have been estimated thanks to the following equation:

$$B_{eff}^2 = B_{hf}^2 + B_{app}^2 - 2B_{hf}B_{app}cos\theta$$

Where B_{hf} is the hyperfine field, B_{eff} the total effective magnetic field at the nucleus, B_{app} the external applied magnetic field and α is the angle between B_{eff} and B_{app}.

The angle θ corresponds to the canting angle for the octahedral sites whereas for the tetrahedral ones, the canting angle is equal to π- θ. This is because of the relative arrangement of the hyperfine and applied fields vectors that are parallel or antiparallel aligned for tetrahedral or octahedral sites, respectively.

Sample	**Sites**	**B_{app} (T)**	**B_{Hf} (T)**	**$\Delta(B_{Hf})$ (T)**	**B_{eff} (T)**	**$\Delta(B_{eff})$ (T)**	**B_{Hf}^2 (T)**	**$\Delta(B_{Hf}^2)$ (T)**	**B_{eff}^2 (T)**	**$\Delta(B_{eff}^2)$ (T)**	**B_{app}^2 (T)**	**cosα**	**Δ(cosα)**
CoFe_Zn0	Fe T_d	6	52.6	0.3	58.7	0.1	2767	32	3446	12	36	1.01	0.08
	Fe O_h	6	55.2	0.3	49.4	0.1	3047	33	2440	10	36	0.96	0.09
CoFe_Zn0.30	Fe T_d	6	52.7	0.3	59.1	0.1	2777	32	3493	12	36	1.06	0.08
	Fe O_h	6	54.1	0.3	48.1	0.1	2927	32	2314	10	36	1.00	0.09
CoFe_Zn0.46	Fe T_d	6	52.3	0.3	59.1	0.1	2735	31	3493	12	36	1.12	0.08
	Fe O_h	6	53.8	0.3	47.7	0.1	2894	32	2275	10	36	1.02	0.09
CoFe_Zn0.53	Fe T_d	6	52.2	0.3	58.9	0.1	2725	31	3469	12	36	1.10	0.08
	Fe O_h	6	53.6	0.3	47.8	0.1	2873	32	2285	10	36	0.96	0.09

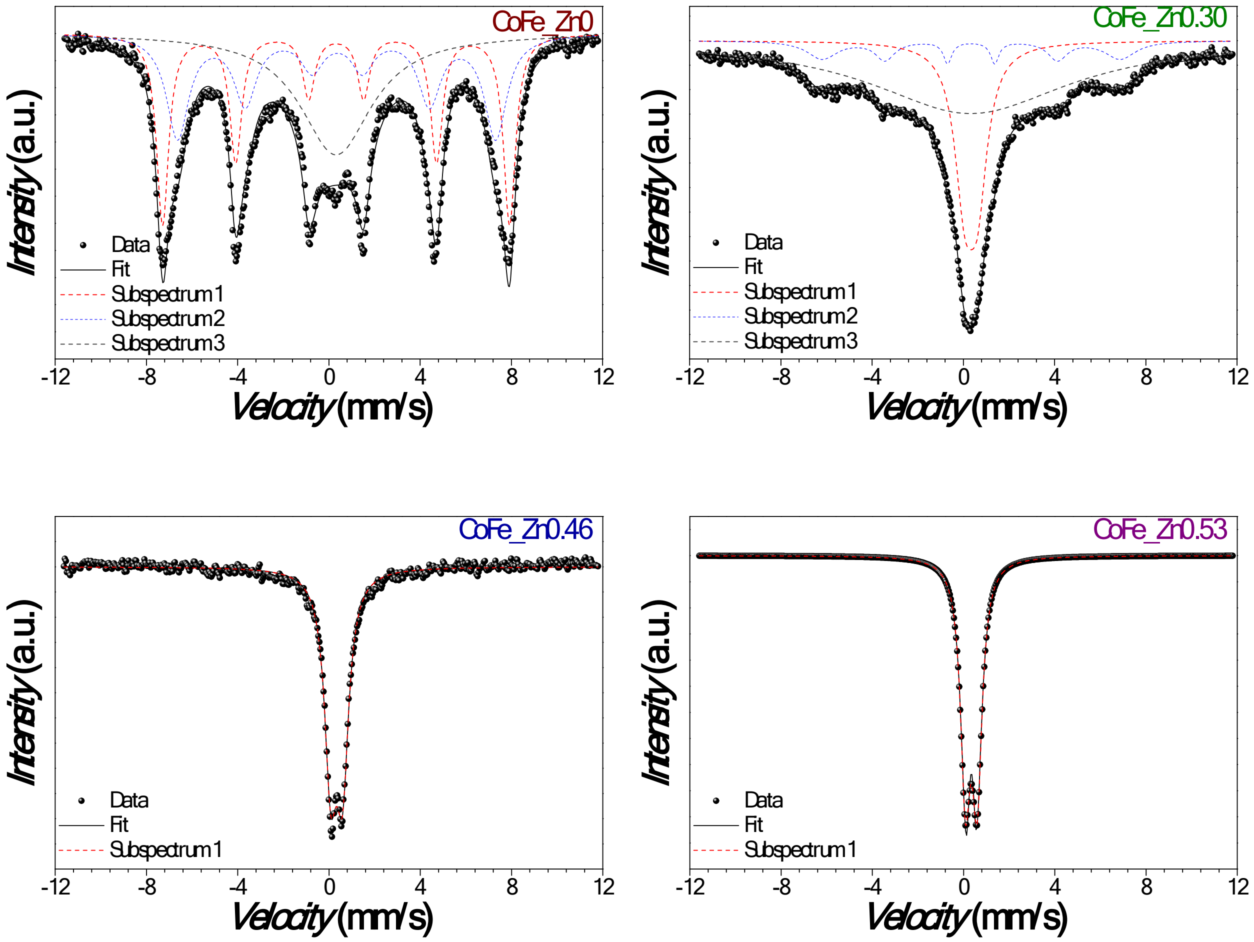

Figure S7. Room temperature Mössbauer spectra of the samples CoFe_Zn0, CoFe_Zn0.30, CoFe_Zn0.46, CoFe_Zn0.53.

2. Estimation of Néel relaxation time

Curve fitting for the estimate of Néel relaxation time at 300 K, τ_N, by the Vogel-Fulcher model $\tau_N = \tau_0 exp\left(\frac{E_b}{T - T_0}\right)$, where τ_0 is the characteristic relaxation time, E_b is the energy barrier against the magnetisation reversal, T is the absolute temperature and T_0 is the temperature value accounting for the strength of magnetic interactions.

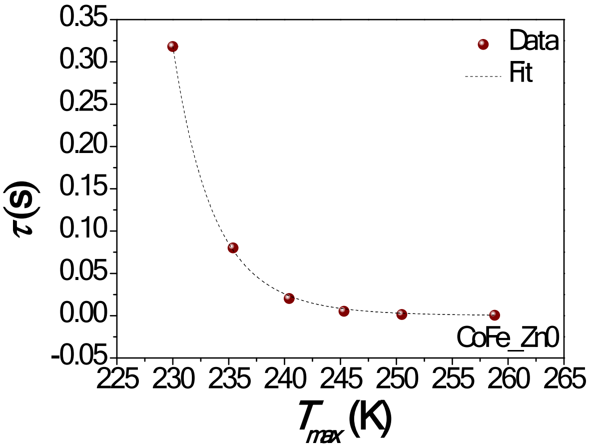

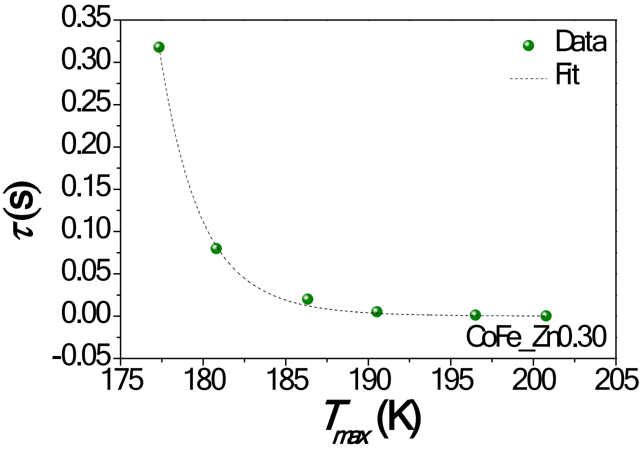

Sample	**τ_0 (s)**	**E_b(K)**	**T_0 (K)**	***τ_N (s)***	***f_{max} (Hz)***
CoFe_Zn0	$4.8\ 10^{-13}$	2672.2	131.8	$3.8\ 10^{-6}$	$4.2\ 10^{4}$
CoFe_Zn0.30	$4.8\ 10^{-14}$	2142.0	104.8	$2.8\ 10^{-9}$	$5.7\ 10^{7}$

References

1. D. Peddis, N. Yaacoub, M. Ferretti, A. Martinelli, G. Piccaluga, A. Musinu, C. Cannas, G. Navarra, J. M. Greneche, and D. Fiorani, *J. Phys. Condens. Matter*, 2011, **23**, 426004.
2. E. Fantechi, G. Campo, D. Carta, A. Corrias, C. de Julián Fernández, D. Gatteschi, C. Innocenti, F. Pineider, F. Rugi, and C. Sangregorio, *J. Phys. Chem. C*, 2012, **116**, 8261–8270.
3. V. Blanco-Gutiérrez, J. A. Gallastegui, P. Bonville, M. J. Torralvo-Fernández, and R. Sáez-Puche, *J. Phys. Chem. C*, 2012, **116**, 24331–24339.
4. D. Varshney, K. Verma, and A. Kumar, *J. Mol. Struct.*, 2011, **1006**, 447–452.
5. B. P. Ladgaonkar and A. S. Vaingankar, *Mater. Chem. Phys.*, 1998, **56**, 280–283.
6. E. Wolska, E. Riedel, and W. Wolski, *Phys. Status Solidi*, 1992, **132**, K51–K56.
7. G. V. M. Jacintho, A. G. Brolo, P. Corio, P. A. Z. Suarez, and J. C. Rubim, *J. Phys. Chem. C*, 2009, **113**, 7684–7691.
8. C. Cannas, A. Musinu, A. Ardu, F. Orrù, D. Peddis, M. Casu, R. Sanna, F. Angius, G. Diaz, and G. Piccaluga, *Chem. Mater.*, 2010, **22**, 3353–3361.
9. L. Zhang, R. He, and H.-C. Gu, *Appl. Surf. Sci.*, 2006, **253**, 2611–2617.
10. D. Peddis, C. Cannas, A. Musinu, A. Ardu, F. Orrù, D. Fiorani, S. Laureti, D. Rinaldi, G. Muscas, G. Concas, and G. Piccaluga, *Chem. Mater.*, 2013, **25**, 2005–2013.
11. M. Klokkenburg, J. Hilhorst, and B. H. Erné, *Vib. Spectrosc.*, 2007, **43**, 243–248.
12. W. B. White and B. A. DeAngelis, *Spectrochim. Acta Part A Mol. Spectrosc.*, 1967, **23**, 985–995.
13. S. Ayyappan, G. Paneerselvam, M. P. Antony, and J. Philip, *Mater. Chem. Phys.*, 2011, **128**, 400–404.
14. S. Ayyappan, G. Gnanaprakash, G. Panneerselvam, M. P. Antony, and J. Philip, *J. Phys. Chem. C*, 2008, **112**, 18376–18383.
15. G. Gnanaprakash, J. Philip, T. Jayakumar, and B. Raj, *J. Phys. Chem. B*, 2007, **111**, 7978–7986.
16. G. A. van Ewijk, G. J. Vroege, and A. P. Philipse, *J. Magn. Magn. Mater.*, 1999, **201**, 31–33.